

6. Pimm, S. L., Russell, G. J., Gittleman, J. L. and Brooks, T. M., *Science*, 1995, **269**, 347–350.
7. Palmer, M. W., *Ecology*, 1990, **71**, 1195–1198.
8. Soberon, M. J. and Llorente, B. J., *Conserv. Biol.*, 1993, **7**, 480–488.
9. Weiher, E., *J. Ecol.*, 1999, **87**, 1005–1011.
10. Wilson, J. B. and Chiarucci, A., *J. Veg. Sci.*, 2000, **11**, 773–775.
11. Crawley, M. J. and Harral, J. E., *Science*, 2001, **291**, 864–868.
12. Huber, R., *Appl. Veg. Sci.*, 1999, **2**, 257–266.
13. McCune, B. and Mefford, M. J., *PC-ORD Multivariate Analysis of Ecological Data*, version 4, MjM Software Design, Oregon, USA, 1999.
14. SPSS, *SPSS Base 7.5 Applications Guide*, SPSS Inc, Chicago, 1997.
15. Williams, C. B., *Nature*, 1943, **152**, 264–267.
16. Connor, E. F. and McCoy, E. D., *Am. Nat.*, 1979, **113**, 791–833.
17. Taylor, D. R., Aarssen, L. W. and Loehle, C., *Oikos*, 1990, **58**, 239–250.
18. Ericksson, O., *Oikos*, 1993, **68**, 371–374.
19. Oksanen, J., *J. Ecol.*, 1996, **84**, 293–295.
20. Harte, J., Kinzig, A. and Green, J., *Science*, 1999, **284**, 334–336.
21. Hill, M. O., *J. Veg. Sci.*, 2001, **12**, 143–144.
22. Jha, C. S. and Singh, J. S., *J. Veg. Sci.*, 1990, **1**, 609–614.
23. Verma, D. M., Pant, P. C. and Hanfi, M. I., *Flora of Raipur, Durg and Rajnandgaon*, Botanical Survey of India, Howrah, 1985.

ACKNOWLEDGEMENT. Financial support from the Ministry of Environment and Forests, Govt. of India is acknowledged.

Received 5 December 2002; revised accepted 11 February 2003

Halocarbon mineralization and catalytic destruction by metal nanoparticles

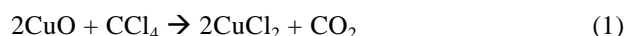
A. Sreekumaran Nair and T. Pradeep*

Department of Chemistry and Regional Sophisticated Instrumentation Centre, Indian Institute of Technology Madras, Chennai 600 036, India

Halocarbons undergo catalytic destruction and mineralization with silver and gold nanoparticles in solution forming metal halides and amorphous carbon. The reaction, studied for several halocarbons and one chlorofluorocarbon, is efficient and complete destruction occurs within several hours at room temperature. The methodology can be applied for detection, destruction and removal of halocarbons with complete recovery of the products, implying possible applications.

HALOCARBON stockpile on the Earth's surface is massive and efficient destruction strategies are intensely pursued. Chlorocarbons are some of the major pollutants of soil

and water and their detection in trace quantities as well as removal at these levels constitute important aspects of research. Many of them are toxic, mutagenic and resistant to microbial degradation. Chlorofluorocarbons, being inert in the troposphere reach the stratosphere and contribute to the catalytic destruction of ozone. Various methodologies for the destruction of halocarbons have been proposed^{1–5}; reductive dehalogenation and mineralization are of particular relevance here. In mineralization, a recent approach³ is the use of sodium oxalate to generate sodium halides from halocarbons. Halocarbon degradation by activated carbon⁴ has been demonstrated. Most recent approach⁵ in this direction is the reaction,



using metal oxide nanoparticles.

In this paper, we report a promising and novel reaction of metal nanoparticles, which bring about halocarbon mineralization efficiently, economically and eco-friendly. The reaction, studied with silver and gold nanoparticles, results in the catalytic destruction of halocarbons forming silver halide (gold chloride) and amorphous carbon. The reaction is more efficient with silver nanoparticles. Reaction is efficient for all particles in the size range of 2–150 nm. It is not observed for bulk metals and therefore constitutes one of the examples of size selective reactivity of nanoparticles. We believe that this promising reaction is one of the best methods to mineralize halocarbon stockpile on the earth's surface.

Our experiments were conducted with several kinds of nanoparticles prepared using well-established procedures. Gold and silver particles in the 10–150 nm range were prepared by the citrate reduction route⁶ and were characterized by optical absorption spectroscopy (UV-visible, Perkin Elmer Lambda 25) and transmission electron microscopy (TEM, 120 KV, Philips CM12). Au and Ag particles with thiolate capping were prepared by the Brust procedure⁷ and were characterized in the as-prepared form as well as after-size separation (solvent selective precipitation) by a variety of techniques⁸. Particles in the size range of 2–150 nm were accessible by these two procedures. Some of the studies were also done using TiO₂ and ZrO₂ covered core-shell nanoparticles of Au and Ag, prepared using a single-step procedure⁹. Identification and quantitation of the reaction products were done using X-ray diffraction (XRD, Shimadzu XD-D1, CuK α), gas chromatography (GC, HP 5987), infrared spectroscopy (FT-IR, Perkin Elmer Spectrum One) and mass spectrometry (MS, Balzers Thermostar).

Majority of the experiments were performed with citrate capped silver clusters. In a typical procedure¹⁰, 25 ml of 0.005 M stock solution of silver nitrate in water is diluted to 125 ml and heated until it begins to boil. 5 ml of 1% sodium citrate solution is added and heating continued till the colour change was evident (yellow). The

*For correspondence. (e-mail: pradeep@iitm.ac.in)

average particle size was 60–80 nm (ref. 10). To 2.5 ml of 1 : 1 (by volume) mixture of the nanoparticle solution and 2-propanol, 50 μ l of CCl_4 was added and kept aside for observation by UV-visible spectroscopy. 2-propanol was added to increase miscibility of CCl_4 (solubility of $\text{CCl}_4 = 0.65 \text{ mg}/100 \text{ g}$ at 298 K in water) in most of the experiments. Reaction occurs in methanol and ethanol solutions as well, with different kinetics. Figure 1 shows change in the absorption spectrum of this solution as a function of the reaction time showing the complete disappearance of the plasmon peak at 438 nm within a time interval of 12 h. No significant shift in the peak position was observed but as the reaction proceeds, certain change in the absorption profile was observed, presumably as a result of changes in particle morphology (TEM showed elongated particles, see below). The solution gradually became colourless as shown at the end of the reaction (inset). A grey solid precipitated; the precipitation can be accelerated by centrifuging. Powder XRD of the precipitate (Figure 2a) matched exactly with AgCl^{11} (Figure 2b) and no metallic silver reflections of the parent nanoparticles were found suggesting complete conversion (no free Ag^+ was present in the solution). Grey appearance of the solid was due to the presence of amorphous carbon with the precipitated AgCl , the former did not show any diffraction. AgCl was dissolved in dilute ammonia and the solution answered the characteristic tests for Ag^+ .

The material after AgCl removal showed a sharp infrared feature at 1384 cm^{-1} characteristic of amorphous carbon

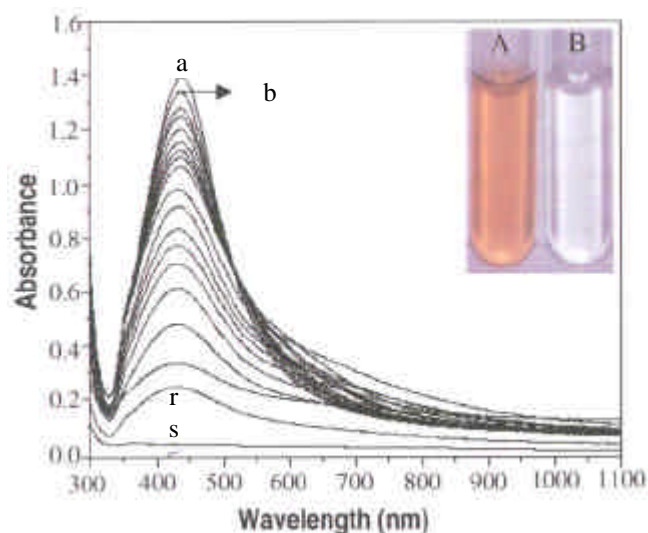


Figure 1. Variation of the UV-visible absorption spectrum of silver clusters (total silver concentration of 0.001 M) upon addition of CCl_4 . Spectrum of the pure cluster solution (a) shows the plasmon at 438 nm characteristic of silver nanoparticles of 60–80 nm diameter. Trace (b) was taken just after the addition of 50 μ l of CCl_4 to 2.5 ml of the solution. Subsequent traces were taken at the interval of 30 min (c to r) and (s) was recorded after 12 h showing the complete disappearance of the plasmon. Inset shows the picture of the nanoparticle solution (A) and the reaction product (B) after adding CCl_4 (12 h).

materials¹². All the CCl_4 features disappeared from the spectrum and no intensity was seen in the C-Cl stretching range (the spectra are given in the supporting information (1)). The material burned completely in air giving CO_2 . FT-Raman spectrum of the material confirmed that it is composed of amorphous carbon (spectrum is given in supporting information (2)). The G band and D band of the amorphous carbon centered at 1550 and 1288 cm^{-1} respectively are seen¹².

The solution after separation of the precipitate contained free chloride ions, which was quantitated by precipitation. CCl_4 was not detected in the citrate solution left behind (by gas chromatography). No new organic product was detected in GC. *In situ* infrared spectroscopy revealed the gradual disappearance of C-Cl stretching frequency and the evolution of amorphous carbon, and no additional feature was detected. Possibility of CO_2 formation was suspected (due to oxidation of carbon) as the solution contained dissolved air, and the gas volume above the reaction vessel was analysed by mass spectrometry and no new species were detected. There was a drastic change in the pH of the solution during the reaction, which changed from 9.7 (nanoparticle solution) to 1.2 (after the reaction). On the basis of all these experiments, we conclude that the reaction observed is a catalytic decomposition of halocarbons. A balanced equation cannot be given for the above reaction because of the ambiguity in the value of the number of atoms in a given metal cluster. The electrons are supplied by the solvent, presumably by the reaction,

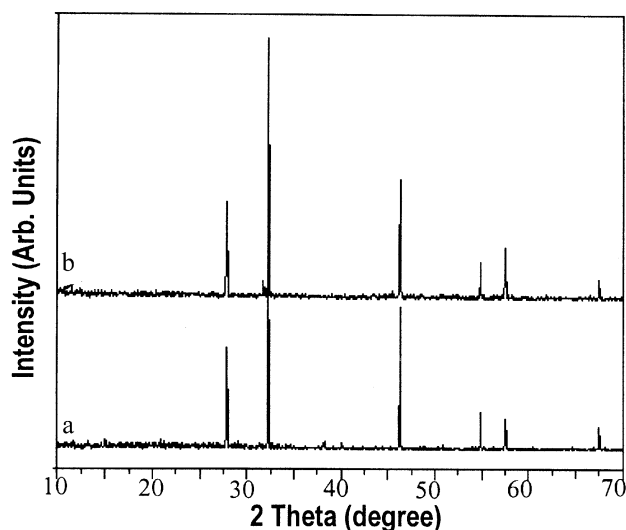
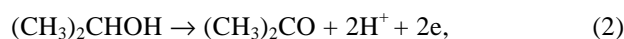


Figure 2. A comparison of the powder diffractograms of (a) CCl_4 reaction product with silver nanoparticles and (b) AgCl prepared by adding Ag^+ to a dilute solution of Cl^- . The diffractogram matches exactly with the powder diffraction data file. No features for carbon are seen in XRD, confirming the amorphous nature of it.

which explains the increase in pH, though $(\text{CH}_3)_2\text{CO}$ was not detected due to reduced concentrations. The pH was considerably higher (3.5) and the reaction was slower in a solution containing acetonitrile or acetone (instead of 2-propanol). Reaction conducted under quantitative conditions showed destruction of 19 CCl_4 molecules per silver atom. This number varied with the preparation conditions, indicating variation of the catalytic properties with size. In pure water medium, the reaction did not lead to the precipitation of AgCl and amorphous carbon as CCl_4 solubility is low (see below).

The direct mineralization reaction,



is nearly thermoneutral, using the enthalpy values of materials in their stan^o₂₉₈ for CCl_4 and AgCl are, -128.2 and $-127.01.2 \text{ kJ mol}^{-1}$ respectively, making H of the reaction to be 1.2 kJ mol^{-1} ¹³. Reaction enthalpies for other chloromethanes are also not large. When acetonitrile was used instead of 2-propanol, eq. (3) was nearly quantitative. As the metal involved is of nanodimension with excess energy than the bulk, reaction (3) is expected to be exothermic. Thus, nanodimension and the energetic surface atoms are believed to help in overcoming the thermochemical and entropic barriers in bringing about the above mineralization reaction.

Interaction of CCl_4 and O_2 with silver nanoparticles leading to oxidation of silver has been reported before¹⁴ leading to a red shift of the plasmon excitation. CCl_3 -induced destruction of metal core happens in the case of thiolate protected nanoparticles in toluene medium¹⁵. Complete destruction as reported here has not been observed till now. Catalytic destruction has to be a cumulative effect of several processes. Although the details of the processes at the nanoparticle surface are not clearly known, it appears that three events occur, namely (1) catalytic decomposition of CCl_4 at the nanoparticle surface, (2) metal-assisted decomposition of halocarbons or net mineralization and metal corrosion, (3) an oxidation reaction involving the solvent releasing protons (and electrons). It is clear that (2) happens independently, while (1) and (3) are coupled.

Several other halocarbons exhibited the reaction. Reactivity was checked with common halocarbons such as, CH_2Cl_2 , CHBr_3 and $\text{C}_6\text{H}_5\text{CH}_2\text{Cl}$ (benzyl chloride) and 3-bromo 1-propyne. We also checked a chlorofluorocarbon, namely CCl_3F , and the reaction was similar to that of CCl_4 . The C–F bond completely disappeared and amorphous carbon was formed. No C–H frequency was detected in the carbon product of CH_2Cl_2 and CHCl_3 . The fastest reaction observed was with bromoform. Silver bromide was precipitated within 10 min of mixing the two solutions.

No reaction was observed with a silver mirror made with Tollen's reagent even after refluxing, which shows

that this reaction is characteristic of particles in the nano regime. The reaction was seen to occur with a range of cluster materials, citrate capped clusters, thiolate capped nanocrystals (with benzyl chloride) and oxide protected metal particles⁹. However, in very large particles (made by increasing metal ion concentration), no reaction was seen, the particles agglomerated and precipitated upon addition of CCl_4 . The aggregates could be brought back to solution by sonication, but no reaction was observed.

The reaction with gold nanoparticles was slower and complete mineralization was observed over a period of 48 h (Figure 3). The plasmon red shifted upon the addition of halocarbons (benzyl chloride), which could be due to the adsorption of halocarbons on the surface of gold nanoparticles and the change in colour was distinct. After 12 h, the particles precipitated. Shape changes, mostly to elongated particles, are observed in transmission electron microscopy, which explained the changes in the plasmon structure¹⁶. Upon stirring, reaction continued and complete mineralization occurred resulting in the formation of AuCl_3 (see supporting information 3). Thermochemistry suggests a more endothermic^o₂₉₈ for $\text{AuCl}_3 = -117.6 \text{ kJ mol}^{-1}$ which could be the reason for the observed change. An abrupt reaction was observed with Cu nanoparticles in agreement with thermochemis^o₂₉₈ $= -220.1 \text{ kJ mol}^{-1}$.

It is important that the method is applicable to dilute solutions so that applications in water purification become

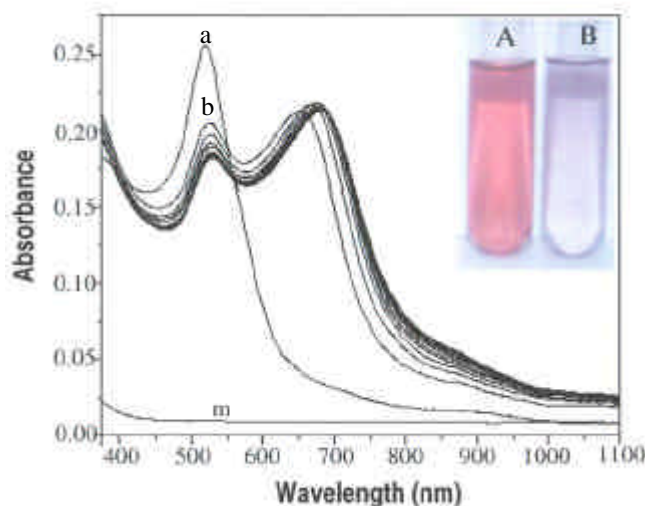


Figure 3. Variation of the UV-visible absorption spectrum of gold clusters upon addition of benzyl chloride. Spectrum of pure cluster solution (a) shows the plasmon at 521 nm characteristic of 15–20 nm gold particles. Trace (b) was recorded just after adding 50 μl benzyl chloride to 2.5 ml of cluster solution. Subsequent traces were recorded at 20 min intervals. The plasmon red shifts to 681 nm initially upon addition and it disappears completely after 48 h (m). Inset shows pictures of the nanoparticle solution (A) and the reaction product (B) after adding benzyl chloride (after 1 h).

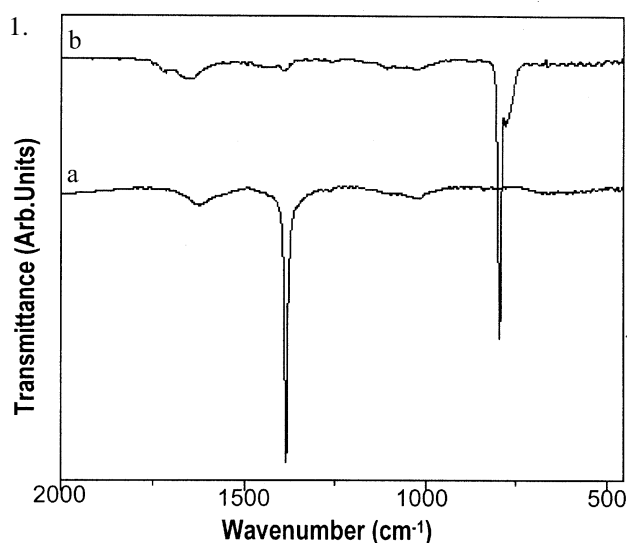
possible. Saturated solutions of halocarbons (CH_2Cl_2 , CHCl_3 and CCl_4) were prepared in water and citrate stabilized silver clusters were added (without 2-propanol). After stirring for 2 h, the halocarbon levels went below the detection limit in both GC and MS. The reaction appears to be a direct mineralization process.

In all the cases investigated, the mineralization was complete and the reaction products were removed completely from solution. Silver chloride being a secondary ore of silver, the material may be recycled to get pure Ag, thus making it a zero waste reaction. The process could be conducted in an eco-friendly manner with excellent efficiency. For drinking water applications, it is

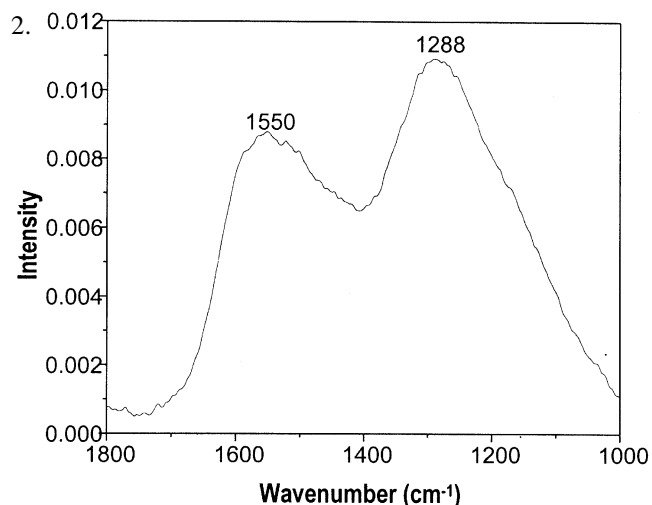
important to remove the ions (citrate, nitrate, halide, etc.) by ion exchange.

In conclusion, we have found a novel reaction by which halocarbons are mineralized by metal nanoparticles. The reaction in presence of alcohols is a catalytic destruction leading to the metal halide and amorphous carbon. The reaction occurs with fluoro, chloro and bromocarbons. The reaction products can be removed completely from the solution, suggesting a viable process for halocarbon removal. Application of this reaction in the detection, extraction and degradation of environmentally significant halocarbons in general, and pesticides in particular, is being pursued currently.

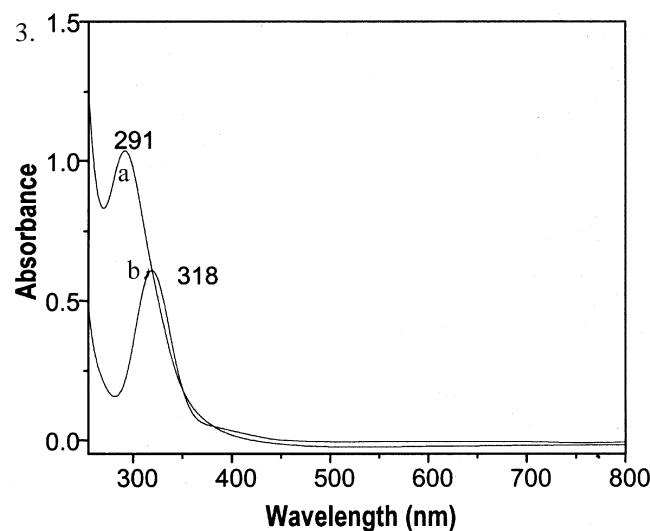
Supporting information



1. FTIR spectra of (a) CCl_4 reaction production in KBr matrix and (b) CCl_4 in the liquid state. The reaction product was treated with diluted NH_3 , washed with nanopure water and dried at 100°C .



2. The Raman spectrum of the amorphous carbon obtained in the reaction between Ag clusters and CCl_4 . The feature at 1550 cm^{-1} corresponds to G band and that at 1288 cm^{-1} corresponds to D band of amorphous carbon¹².



3. The UV-visible spectra showing the emergence of AuCl_3 peak in the reaction between Au citrate and benzyl chloride. (a) UV-visible spectrum of $\text{H[AuCl}_4\text{]}\cdot 3\text{H}_2\text{O}$ in water; (b) Au citrate reaction product with benzyl chloride. The shift in the peak maximum from 291 to 318 is due to the change of solvent (from water to water alcohol (1:1 volume) mixture) and the presence of citrate ions.

1. Matheson, L. J. and Tratnyek, P. G., *Environ. Sci. Technol.*, 1994, **28**, 2045–2053.
2. Petrosius, S. C., Drago, R. S., Young, V. and Grunewald, G. C., *J. Am. Chem. Soc.*, 1993, **115**, 6131–6137.
3. Burdeniuc, J. and Crabtree, R. H., *Science*, 1996, **271**, 340–341.
4. Nicoll, G. and Francisco, J. S., *Environ. Sci. Technol.*, 1999, **33**, 4102–4106, and the references cited therein.
5. Chien, Y. C., Wang, H. P. and Yang, Y. W., *Environ. Sci. Technol.*, 2001, **35**, 3259–3262.
6. Enustun, B. V. and Turkevich, J., *J. Am. Chem. Soc.*, 1963, **85**, 3317–3328.
7. Brust, M., Walker, M., Bethel, D., Schiffrin, D. J. and Whyman, R., *J. Chem. Soc., Chem. Commun.*, 1994, 801–802.
8. Sandhyarani, N. *et al.*, *Chem. Mater.*, 2000, **12**, 104–113; Sandhyarani, N. and Pradeep, T., *Int. Rev. Phys. Chem.*, 2003, **22**, 221–262.
9. Pastoriza-Santos, I. and Liz-Marzan, L. M., *Langmuir*, 1999, **15**, 948–951; Pastoriza-Santos, I., Koktysh, D. S., Mamedov, A. A., Giersig, M., Kotov, N. A. and Liz-Marzan, L. M., *Langmuir*,

- 2000, **16**, 2731–2735; Tom, R. T. *et al.*, *Langmuir*, 2003, **22**, 3439–3445.
10. Kamat, P. V., Flumiani, M. and Hartland, G. V., *J. Phys. Chem.*, 1998, **B102**, 3123–3128.
 11. Powder XRD file 22.
 12. Liu, X. W., Lin, J. H., Hsieh, W. J. and Shih, H. C., *Diamond Related Mater.*, 2002, **11**, 1193–1199.
 13. *Handbook of Chemistry and Physics*, CRC Press, New York, 1999, 80th edn, pp. 5-4–5-60.
 14. Henglein, A., *Chem. Mater.*, 1998, **10**, 444–450.
 15. Sandhyarani, N., Pradeep, T. and Francisco, J. S., *Chem. Phys. Lett.*, 2001, **342**, 272–276.
 16. Link, S. and El-Sayed, M. A., *J. Phys. Chem.*, 1999, **B103**, 8410–8426.

ACKNOWLEDGEMENTS. The monolayer protected cluster research program of T. P. is funded by the Council of Scientific and Industrial Research. His oxide protected nanoparticle program is funded by the Ministry of Information Technology.

Received 24 March 2003; accepted 11 June 2003

Association of vitamin D receptor gene variants of *BsmI*, *ApaI* and *FokI* polymorphisms with susceptibility or resistance to pulmonary tuberculosis

P. Selvaraj*, G. Chandra, Sunil Mathan Kurian, A. M. Reetha and P. R. Narayanan

Tuberculosis Research Centre, Indian Council of Medical Research, Chennai 600 031, India

Vitamin D receptor (VDR) gene polymorphism was studied to find out whether the variants of this gene are associated with susceptibility or resistance to pulmonary tuberculosis (PTB) and bacteriological relapse of tuberculosis. *BsmI*, *ApaI* and *FokI* polymorphisms of VDR gene were studied in PTB patients ($n = 120$), patient contacts (spouses of the patients; $n = 80$), bacteriological relapse patients ($n = 48$) and quiescent patients ($n = 48$). Significant increase of *Bb* genotype (heterozygote carrier) of *BsmI* polymorphism ($P = 0.028$) and *FF* genotype (homozygotes of common allele *F*) of *FokI* polymorphism ($P = 0.034$) were observed in male PTB patients than male contacts. The *BB* genotype (homozygote of common allele *B*) of *BsmI* polymorphism and *AA* genotype (homozygote of common allele *A*) of *ApaI* polymorphism were increased in male contacts than male PTB patients (*BB*: $P = 0.018$; *AA*: $P = 0.04$). No significant differences were found among female patients and female contacts. In bacteriological relapse cases of

PTB, a decreased frequency of *AA* genotype ($P = 0.015$) and an increased frequency of *Aa* genotype ($P = 0.024$) were observed in bacteriological relapse patients than quiescent patients of PTB. The present study suggests that *Bb* genotype of *BsmI* polymorphism and *FF* genotype of *FokI* polymorphism of VDR gene may be associated with the susceptibility to tuberculosis in males. The *BB* and *AA* genotypes may be associated with resistance to PTB in males. The genotype *Aa* may be associated with bacteriological relapse and *AA* may be associated with protection against bacteriological relapse.

VITAMIN D₃ (1,25 dihydroxy vitamin D₃), the active form of vitamin D regulates calcium and bone metabolism. It is an immunoregulatory hormone which plays a vital role in monocyte/macrophage activation and is shown to influence the immune response¹. Vitamin D₃ is one of the few mediators shown to impair the growth of *Mycobacterium tuberculosis* in the macrophage². The effects of vitamin D are exerted by interaction through vitamin D receptor (VDR). Various diallelic polymorphisms have been identified in the VDR gene (*BsmI* site – alleles *B* [common allele] and *b* [infrequent allele]; *ApaI* site – alleles *A* [common allele] and *a* [infrequent allele]; *TaqI* site – alleles *T* [common allele] and *t* [infrequent allele]; *FokI* site – alleles *F* [common allele] and *f* [infrequent allele])^{3–9}. Among these polymorphisms, *BsmI* and *TaqI* are shown to be associated with the bone mineral density^{6,10}. The *tt* genotype of the infrequent allele of *TaqI* polymorphism of VDR gene has been shown to be associated with decreased bone mineral density, resistance to primary and secondary hyperthyroidism, and resistance to prostatic cancer^{3,6,7}. The variant genotype *aa* (homozygotes of infrequent allele) of *ApaI* and *bb* (homozygote of infrequent allele) of *BsmI* polymorphisms of VDR gene have been shown to be associated with increased bone mineral density in females¹⁰, and the VDR haplotypes *Bat* and *baT* with the regulation of VDR expression. Moreover, there seems to be no apparent linkage disequilibrium between these polymorphisms and the VDR *FokI* polymorphism¹¹. By producing a reporter gene construct under the control of a vitamin D response element, increased vitamin D-dependent transcriptional activation of VDR gene was shown with *m* allele (*F* allele of *FokI* polymorphism) than *M* allele (*f* allele of *FokI* polymorphism)¹².

It has been shown that in the north Indian population, *tt* genotype is associated with tuberculoid leprosy and *TT* genotype with lepromatous leprosy¹³. The variant genotype *tt* of VDR gene has been shown to be associated with decreased risk of tuberculosis in Gambian (African) population¹⁴. Our recent studies in south Indian pulmonary tuberculosis (PTB)¹⁵ and spinal tuberculosis (extrapulmonary form of tuberculosis)¹⁶ patients revealed that variant genotype *tt* of VDR is associated with susceptibility to pulmonary as well as spinal tuberculosis in female

*For correspondence. (e-mail: psraj21@hotmail.com)